Mechanical Systems and Signal Processing 215 (2024) 111390

Contents lists available at ScienceDirect

Mechanical Systems and Signal Processing

journal homepage: www.elsevier.com/locate/ymssp

On the strain-sensing capabilities of a novel all-solid-state sodium-based-electrolyte battery under vibration loads

Bruno Guilherme Christoff [a,*], Denys Marques [b,f], João Paulo Carmo [c], Maria Helena Braga [d,e], Volnei Tita [a,f]

[a] Department of Mechanical Engineering, Faculty of Engineering, University of Porto, Porto, Portugal
[b] Department of Mechanical Engineering, Federal Center of Technological Education Celso Suckow da Fonseca, Angra dos Reis, RJ, Brazil
[c] Department of Electrical Engineering, São Carlos School of Engineering, University of São Paulo, São Carlos, SP, Brazil
[d] Department of Engineering Physics, Faculty of Engineering, University of Porto, Porto, Portugal
[e] LAETA - INEGI, Institute of Science and Innovation in Mechanical and Industrial Engineering, Porto, Portugal
[f] Department of Aeronautical Engineering, São Carlos School of Engineering, University of São Paulo, São Carlos, SP, Brazil

ARTICLE INFO

Communicated by J.E. Mottershead

Keywords:
All-solid-state battery
Structural battery
Vibrational test
Strain-sensing

ABSTRACT

Growing environmental concerns and the demand for sustainable resource use have raised questions about the conventional use of lithium-ion batteries. In this context, solid-state sodium-based batteries are considered promising energy storage devices due to their excellent performance, cost-effectiveness, and eco-friendly composition. Despite their unquestionable storage capacity, this new battery type may possess additional functionalities that have not been thoroughly explored in the existing literature. In this study, the application of a novel battery developed by a research group at the University of Porto as a strain-sensing device under vibration loads is demonstrated. This battery is an all-solid-state sodium-ion-based ferroelectric battery, and it is expected to exhibit piezoelectric behaviour. With the goal of potential future applications in self-powered Structural Health Monitoring (SHM) systems, the experimental setup replicates conditions similar to those encountered in damage monitoring of composite structures. The solid-state battery is attached to an aluminium beam, which is clamped to an electrodynamic shaker. The beam-battery system is then subjected to constant-frequency excitation, and the battery's electric potential output is analysed in both time and frequency domains. The filtering of the acquired signal from the battery significantly reduced both the interference and harmonic distortion. The experimental results for the base excitation of 25Hz showed a dominance of the unfiltered 60Hz interference of +14 dB in relation to the unfiltered vibrational signal, while in the filtered situation the amplitude of the vibrational signal was +33 dB above the interference. The same tendency is observed under different frequency excitations. The results indicate that the battery generates a potential difference at the same frequency as that imposed by the shaker. However, its low sensitivity and susceptibility to electromagnetic noise from the electric grid limits the maximum frequency it can effectively monitor. Based on the positive results obtained in the present study, the authors believe that such a device opens up new possibilities for various applications of solid-state batteries, combining their energy storage capabilities with smart sensing functionalities.

* Corresponding author.
E-mail addresses: bchristoff@fe.up.pt (B.G. Christoff), denys.marques@cefet-rj.br (D. Marques), jcarmo@sc.usp.br (J.P. Carmo), mbraga@fe.up.pt (M.H. Braga), voltita@sc.usp.br (V. Tita).

https://doi.org/10.1016/j.ymssp.2024.111390
Received 5 December 2023; Received in revised form 15 February 2024; Accepted 28 March 2024
Available online 13 April 2024

1. Introduction

The rapid increase in global population leads to a series of challenges concerning global warming, energy production and energy storage [1]. This populational growth implies an ever-demanding energy production and storage, without increasing drastically the CO_2 emissions [2]. Batteries have been used to power a wide range of applications, e.g. electric vehicles, and electronic devices [3]. As an environmental concern, the development of new technologies does not focus solely on the reliability and low cost associated with a high energy density in the batteries, but also on eco-friendly materials and processes [4,5]. There is an urgent need to rethink energy usage in all spheres of the global society, and new inexpensive and sustainable energy supply and storage are critical for the sake of future generations [3].

The environmental aspects concerning batteries have long existed and been approached in several ways, and sustainability is now considered as an extra design variable in addition to structure, composition and morphology of new materials [2]. The development, production and use of environmentally friendly batteries are thus key aspects in fulfilling the ever-growing energy demand in an eco-friendly and sustainable way, concerning a future climate-neutral economy with zero-emission mobility goal [6–8].

Lithium-ion batteries (LIBs) are the most widely used battery today, and have dominated the markets of electronic devices, electric vehicles, and many other applications in the past decades [9]. In comparison to other rechargeable battery systems, LIBs exhibit superior performance regarding energy density [3,10–14], and have already demonstrated an exceptional combination of high energy and power density, and long-life [4,15]. However, LIBs have a few drawbacks and limitations, including slow charging, reliance on flammable electrolytes and hazardous materials such as cobalt. In 2018, 64% of cobalt was extracted from just one country, the Democratic Republic of Congo [16]. Moreover, LIBs have cathodes that tend to reach their theoretical capacity limit [6,17] and can seldom withstand more than 1000 cycles [16]. Additionally, in some aspects, their usage and manufacturing are not ideal [2] since LIBs cannot be used above 40 °C due to thermal runaway and, consequently, battery explosion following by the release of toxic electrolyte derivatives [17–19]. Another concern is the high cost and the shortage of lithium resources [6,10], which are inhibiting the application of LIBs mainly in large-scale energy storage systems [9]. To reduce the cost of renewable energy storage, the development of alternative technologies with more economical advantages and better performance is crucial [3,11,20]. Given the ever-growing demand for energy, the limitations of LIBs make this power source unfeasible from both cost and environmental perspectives [21].

As an alternative to LIBs, solid-state electrolytes (SSEs) have been attracting attention due to advantages such as non-flammability, no leakage risk, and better mechanical properties [4,22], the latter being an interesting feature for the use of SSEs as structural batteries. Among SSEs, Sodium-ion batteries (NIBs) are the closest technology in comparison to the well-established LIBs [23]. In addition, since both Lithium and Sodium are Alkali metals, they share similar chemical properties and hence their fundamental principles are identical [10]. This type of battery is also regarded as the next generation of batteries [9], and due to the solid-state electrolyte used, rather than a conventional liquid organic electrolyte, it exhibits better thermal and chemical stability, less flammability, and better durability [24,25]. Another critical aspect in favour of NIBs is the abundance of sodium in Earth's crust [6,26], which ultimately reduces the cost of producing NIBs compared to LIBs [9,27,28]. Besides, it has been shown that with no conventional cathode and anode needed, solid electrolytes based on sodium are ideal for structural battery applications [6,15,29].

In practical applications, these devices have the potential to function as sensors, particularly when ferroelectric properties are detected in certain cases [30]. In this context, Structural Health Monitoring (SHM) is a valuable practice for reducing the frequency of maintenance inspections and for maximising the time between inspections [31,32].

Vibration-based methods are among the most widely used and efficient techniques in SHM [33]. These methods are especially attractive for monitoring damage due to their simple setup and cost-effectiveness, particularly when employed to detect damage in composite structures [34]. In recent literature, significant attention has been directed towards the creation of autonomous (SHM) systems that possess self-sustaining capabilities [35], primarily leveraging piezoelectric transducers for this purpose [36–38]. Nonetheless, the process of harvesting and converting mechanical energy may fall short in delivering the requisite power to fully support an SHM system [39–41], thereby necessitating continued dependence on an external power source such as batteries.

Given this prevailing scenario, the significance of developing self-powered SHM systems with self-sufficient power becomes increasingly apparent. Consequently, numerous scientific endeavours have focused on the innovation of novel multifunctional batteries. Notably, researchers from the Faculty of Engineering at the University of Porto (FEUP - Portugal) have introduced pioneering batteries engineered from multifunctional materials [17].

The FEUP research team has developed solid-state ferroelectric electrolytes, serving as the fundamental building blocks of these groundbreaking batteries. This inherent characteristic endows the electrolyte with piezoelectric properties, signifying substantial potential for deployment as a structural damage sensor within SHM systems. Considering the aforementioned environmental and economic aspects, and the potential of using NIBs as structural batteries, it is safe to assume that this technology has great potential in several engineering applications, such as in vehicles, drones, aeroplanes, etc. Another significant implication that the use of NIBs may provide in the future is the possibility of reaching more efficient and eco-friendly alternatives to energy storage, and as they can be used as structural batteries, this may be an appealing technological solution to reduce the weight, volume, and consumption of electric vehicles and devices [15].

The present work investigates the potentialities of using a novel all-solid-state sodium-ion-based ferroelectric structural battery as a strain-sensing device under vibration loads. The pair of electrodes used are Zinc (−) and Copper (+). Vibrational tests are performed using this battery coupled to an aluminium beam loaded using a shaker. The battery signal variation is obtained when the battery is subjected to constant vibration. This type of test seeks to understand the potential of applying this type of battery as a sensor, which can be very promising in several engineering applications.

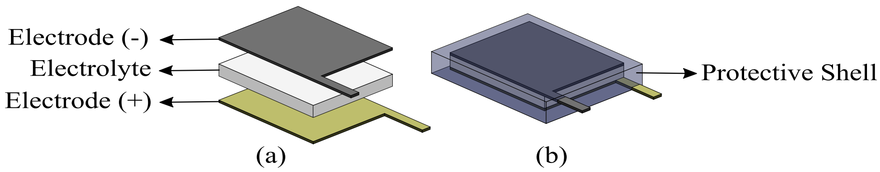

Fig. 1. Schematics of the all-solid-state battery: (a) electrodes (Zinc (−) and Copper (+)) and sodium-based electrolyte; (b) battery assembly and protective polymeric shell.

First, the batteries and the experimental setup used to investigate the strain-sensing of the batteries are described. Next, the results of the vibrational tests are presented, where comparisons are made between the signal of the battery and the signal of an accelerometer attached to the same mechanical system, and the battery signal with and without any signal processing. Finally, the potentialities and perspectives of using this type of battery as a sensor are discussed, as well as the technological implications that this technology may have in future engineering.

2. Experimental procedure

2.1. The battery

The battery used during the test is a novel all-solid-state structural battery, developed by a research group at the University of Porto, Portugal [4]. The battery is composed of a sodium-ion-based ferroelectric electrolyte ($Na_{2.99}Ba_{0.005}ClO$), and the pair of electrodes used are Zinc (−) and Copper (+), as depicted in Fig. 1(a).

Additionally, the battery is coated with a polymeric protective film, as shown in Fig. 1(b). The coating prevents possible contact of the electrolyte with the atmosphere, which might potentially absorb moisture and form an alkaline film that might react with the electrodes, especially with Zinc. Thus, on the one hand, the lifespan of the battery is fully linked to the life span of the protective film. Because, if the polymeric film fails, the battery will fail, as well. On the other hand, the thickness of the film is very thin, and there is no influence on the behaviour of the battery. The battery is comprised of only one cell of 2×2 cm^2 (efficient surface area) and the electrolyte was impregnated on a cellulose membrane with a total thickness of 1 mm. The open circuit voltage of the cell was 1.0 V.

The battery contains a ferroelectric electrolyte, which is a type of dielectric material that polarises spontaneously. Ferroelectric materials configure a reduced group of materials that are also piezoelectric, pyroelectric, and dielectric; in other words, the small number of materials that are ferroelectric must be pyroelectric, piezoelectric, and dielectric; this latter class is the wider containing all the other: dielectric > piezoelectric > pyroelectric > ferroelectric. Besides the properties shown herein, this particular ferroelectric electrolyte, $Na_{2.99}Ba_{0.005}ClO$, possesses interesting properties as a ferroelectric summarised in [4]. Therefore, with the piezoelectric properties inherent in the battery, it is expected to generate a potential difference when subjected to mechanical deformation.

2.2. Testing method

To evaluate the battery's potential as a sensor, a dynamic test is being considered. The objective is to experimentally observe the piezoelectric behaviour of the battery, specifically investigating whether the battery generates a potential difference in response to a bending strain. For this study, an experimental setup has been designed, comprising a cantilever beam coupled to an electrodynamic shaker, with the battery directly attached to the beam. In this configuration, the shaker's base excitation is transmitted to the beam under a predefined constant sine wave frequency. The resulting bending strain in the beam due to dynamic excitation is then transferred to the battery. Given the battery's ferroelectric properties, the mechanical deformation applied to it produces a potential difference, which can be read by a data acquisition system and then sent to a computer for post-processing. The schematic of the experimental apparatus is shown in Fig. 2

An arbitrary function generator (AFG) (Minipa MFG-4205C) is set to produce a sine wave of constant frequency, which is directly used to induce the vibrations to an electrodynamic shaker (VEB Robotron-Meßelektronik "Otto Schön"). In all cases, a peak-to-peak voltage of V_{pp} equal to 10 V is used, which corresponds to the maximum output voltage of the AFG. Additionally, a range of different constant frequencies is employed to generate vibrations in the shaker, so the behaviour of the battery under different frequencies can be investigated. The electric signal from the AFG is converted into mechanical excitation by the electrodynamic shaker at the same frequency as the input signal. This dynamic mechanical displacement is subsequently transmitted to a rigid grip designed to function as a clamping device for a cantilever beam.

An aluminium beam, with a geometry of 1.27 mm thickness, 30 mm width, and 150 mm of free length, is clamped to the rigid grip, being subjected to a base excitation condition. The battery is attached to the aluminium beam using a rapid curing, single-component adhesive, which is able to glue the battery close to the clamp device, as shown in Fig. 3. The effective surface area of the battery, composed of the electrodes and electrolyte, is positioned on the beam, while a short portion of the polymeric film extends outside of the beam. Since the protective shell serves solely for protection, it does not provide any kind of influence on the measurements during testing. Additionally, the battery is positioned in the area where the greatest strain occurs along the length

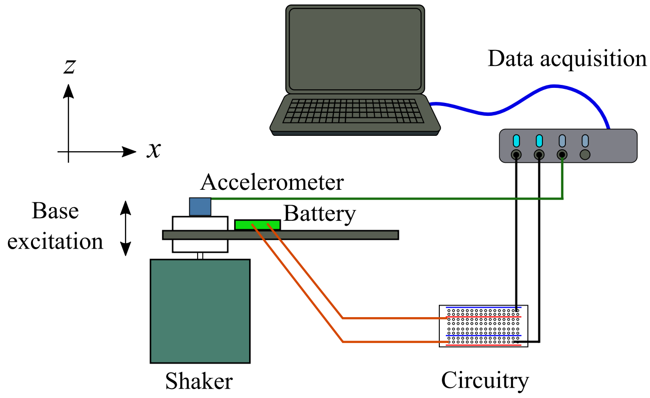

Fig. 2. Set-up of the vibration tests.

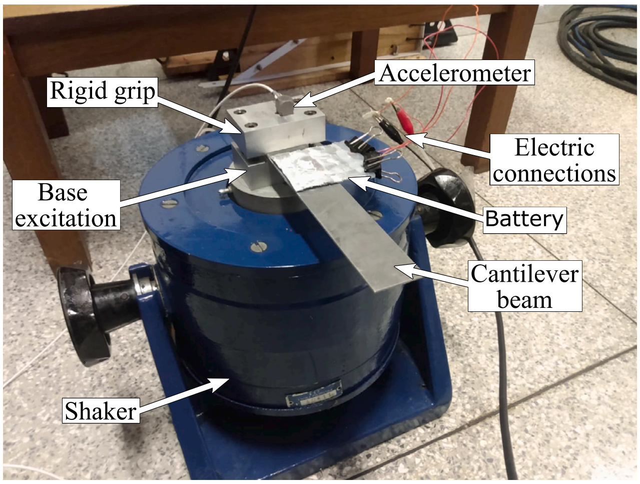

Fig. 3. Depiction of the effective surface area of the battery attached to the aluminium beam mounted to the shaker and accelerometer on the rigid grip.

of the cantilever beam. In the context of structural health monitoring, such as when monitoring damage in composite structures, this closely aligns with real-world applications. In these cases, higher normal stress values come from bending loads, which also promote more significant strains in the longitudinal direction of the structure. It should be noted that the first bending mode of the beam is around 50 Hz, while the second bending mode is found only at 280 Hz. The base-acceleration load is applied in the z-direction (as shown in Fig. 2), and in some tests, an added mass is glued at the free tip of the beam, thus increasing its vibration amplitude.

Electrical connections (Fig. 3) directly linked to the external parts of the battery electrodes (Fig. 1(b)) transmit the generated electrical signal from the battery to a simple circuit mounted directly on a breadboard, designed to remove its DC output voltage while allowing the passage of the voltage oscillations expected to happen during the vibration tests. The electrical voltage is measured by a Kistler LabAmp 5167A data acquisition system [42].

For comparison, an accelerometer (Miniature PiezoBeam Accelerometer Kistler 500 mV/g type 8640A10) is attached to the rigid grip in some tests, to guarantee that the battery generates a signal in the same frequency as the base excitation. The accelerometer signal is also measured by the data acquisition system. Both the battery and accelerometer signals are recorded in a computer in a text format for post-processing.

Fig. 3 shows a photo of the experimental setup employed in the tests, illustrating the transmission of the base excitation from the shaker to the cantilever beam through the rigid grip. Moreover, the positioning of the battery adjacent to the rigid grip and the placement of the accelerometer on the rigid grip are also depicted. It is important to observe that only the effective surface area of the battery, composed of the electrodes and electrolyte, is in contact with the cantilever beam.

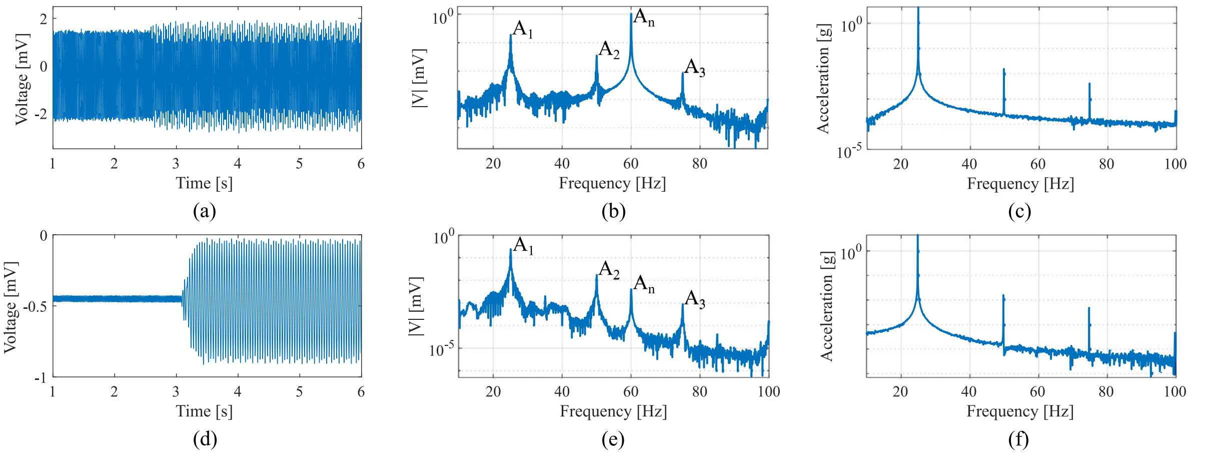

Fig. 4. Signal analyses of the test under a base excitation of 25 Hz: (a) raw battery signal on the time domain; (b) raw battery signal on the frequency domain; (c) accelerometer signal on the frequency domain; (d) filtered battery signal on the time domain; (e) filtered battery signal on the frequency domain; (f) accelerometer signal on the frequency domain.

3. Results and discussion

For all results, the battery behaviour under a constant base excitation of the shaker-beam system is investigated. In all cases, the vibrational test is initiated with the shaker off, and then it is suddenly turned on, and after a few seconds, it is turned off again. Three main aspects are hereby discussed:

(i) the possibility of using the raw signal of the battery to sense strain in a structure;
(ii) the influence of the value of the frequency and the amplitude of the input signal on the battery response; and
(iii) the possibility of using the battery to sense strain in a structure vibrating under higher frequencies.

3.1. Raw signal and filtering

A preliminary study investigates the battery behaviour under a constant base excitation of the system. The frequency of 25 Hz is chosen for the vibrational tests since this frequency is sufficiently distant from the natural frequencies of the shaker-beam system.

The raw signal of the battery on the time domain is shown in Fig. 4(a). It is hard to draw preliminary evaluations about the signal just by analysing this graphic. In addition, no significant change in the battery signal occurs when the shaker is turned on (at around 3 s). The battery signal on the frequency domain is shown in Fig. 4(b). Two signal peaks can be seen at frequencies of 25 Hz, which is the base excitation of the system, and 60 Hz. The analysis on the frequency domain shows that the battery can indeed generate a change in the potential difference in the same frequency of the base excitation, due to the strain caused to the structure. On the other hand, the signal peak at 60 Hz indicates that the battery generates noise due to electromagnetic interference from the electrical network. Additionally, the magnitude of the signal at 60 Hz is higher than at 25 Hz, which might compromise an analysis due to the noise. As a comparison, the accelerometer signal on the frequency domain is shown in Fig. 4(c). It can be seen that the signals of both the battery and the accelerometer have peaks at the same frequencies, except for 60 Hz.

As the shaker is electromagnetic, and several electronic devices are used during the tests, it is expected that the electrical network influences the battery. To reduce this effect without using any type of shielding, the battery signal is processed with an in-built Notch filter to the acquisition system, which is a band-stop filter that attenuates a certain frequency while passing the other frequencies unaltered. The battery signal on the time domain, with the 60 Hz frequency attenuated by the Notch filter, is shown in Fig. 4(d). In that case, a very pronounced difference in the amplitude of the signal can be seen when the shaker is turned off and on, which indicates that the filter used is effective and that the battery can generate a signal at the excitation frequency of the system. On the frequency domain, as shown in Fig. 4(e), one can now see that the signal peak at 25 Hz is higher than at 60 Hz, i.e., the noise due to electromagnetic interference of the electrical network is no longer the main source in the difference of potential generated by the battery.

Again, for comparison, it is used the accelerometer signal during the same test, Fig. 4(f). It is observed by the signal in the frequency domain that the battery identifies the same frequency peaks as the accelerometer, except for the 60 Hz peak, which is not identified by the accelerometer.

For a subsequent comparison, Table 1 shows the results obtained from both the unfiltered and filtered signals for the peak voltage values in the frequency domain. The main peak corresponds to the fundamental frequency of 25 Hz, while the secondary and tertiary peaks are at 50 Hz and 75 Hz, respectively. Additionally, the table includes the amplitude associated with the 60 Hz frequency. The experiment was conducted three times for each case. For tests without filtering in the signal, it is observed that the

Table 1
Peak values of the battery signal in the frequency domain for vibrational tests at 25 Hz.

Status of the acquired signal	Test number	Peak values [mV]			
		25 Hz	50 Hz	60 Hz	75 Hz
Unfiltered	1	0.1965	0.0358	1.0589	0.0085
	2	0.2012	0.0359	1.0663	0.0090
	3	0.1968	0.0363	1.0476	0.0085
Filtered	1	0.2335	0.0167	0.0038	0.0008
	2	0.2059	0.0143	0.0047	0.0007
	3	0.1881	0.0131	0.0046	0.0006

Table 2
Signal-to-noise ratio for vibrational tests at 25 Hz.

Status of the acquired signal	Test number	Signal-to-noise ratio [dB]		
		25 Hz	50 Hz	75 Hz
Unfiltered	1	−14.6259	−29.4107	−41.8333
	2	−14.4849	−29.4364	−41.4541
	3	−14.5212	−29.2018	−41.7148
	$\overline{\text{SNR}}$ ± SD	−14.5439 ± 0.07324	−29.3496 ± 0.1286	−41.6674 ± 0.1939
Filtered	1	35.6545	12.7417	−13.1500
	2	32.7296	9.6179	−16.1727
	3	32.1316	9.0212	−16.9966
	$\overline{\text{SNR}}$ ± SD	33.5052 ± 1.8851	10.4603 ± 1.9981	−15.4398 ± 2.0253

Table 3
Figure-of-merits D_2 and D_3 for vibrational tests at 25 Hz.

Status of the acquired signal	Test number	Secondary peak D2 [Db] at 50 Hz	Tertiary peak D3 [Db] at 75 Hz
Unfiltered	1	−14.7848	−27.2074
	2	−14.9515	−26.9693
	3	−14.6807	−27.1936
Filtered	1	−22.9128	−48.8045
	2	−23.1117	−48.902
	3	−23.1104	−49.1283

absolute voltage values for the frequencies of interest are considerably lower than the signal generated by noise. In contrast, for the filtered signal, the main peak at the fundamental frequency and the secondary peak have higher absolute values than the noise signal.

Furthermore, to compare the level of the desired signals to the level of the noise signal, a signal-to-noise ratio (SNR) is considered, such that

$$\text{SNR} = 20 \log \left(\frac{A_s}{A_n} \right) [\text{dB}] \,, \tag{1}$$

where $A_s, s = 1, 2, 3$ is the amplitude of the signal of interest (in this case, the main peak at 25 Hz and its harmonics at 50 Hz and 75 Hz), and A_n is the amplitude of the noise signal.

Table 2 shows the SNR results for both the filtered and unfiltered battery signals alongside the mean values and standard deviation (SD). In the experimental outcomes for the 25 Hz base excitation, there was a notable prevalence of unfiltered 60 Hz interference at +14 dB compared to the unfiltered battery signal at 25 Hz. Conversely, under the filtered conditions, the amplitude of the battery signal at 25 Hz exceeded the interference by +33 dB. The same pattern is observed for the secondary peak, in which the 60 Hz interference surpasses the unfiltered signal by +29 dB, and for the filtered conditions, the battery signal surpasses the interference by +10 dB. For the tertiary peak, the prevalence of the 60 Hz interference was reduced from +41 dB for the unfiltered battery signal to +15 dB for the filtered battery signal.

The non-linearity inherent to the shaking systems and the supporting cantilever is transmitted into the battery. However, the high sensitivity of this battery working as a transducer allows their detection and quantification. A figure-of-merit D [dB] can quantify the degree introduced by the non-linear components of the oscillating cantilever. This is a numerical indicator and can be defined taking into account the amplitudes A_1 [dB] of the main peak at the fundamental oscillating frequency of 25 Hz with relation to the higher secondary and tertiary peaks A_2 [dB] and A_3 [dB]. These quantities take the form of a spectral distortion and are given by $D_2 = A_2–A_1$ [dB] and $D_3 = A_3–A_1$ [dB]. Table 3 lists the D_2 and D_3, where it is possible to observe that the non-linear component with the higher amplitude is always of at least 20 dB (one order of magnitude or ten times) below the main peak at the fundamental of the vibrational component frequency.

The application of the Notch filter results in a significant reduction of the signal generated at the 60 Hz frequency. In the time domain signal without filtering (Fig. 4(a)), one can observe a change in the signal before and after the shaker is turned on, but it is difficult to distinguish the noise from the signal of interest. On the other hand, when the filter is applied (Fig. 4(d)), it becomes evident that the signal of interest is considerably more prominent when contrasted with the noise. This pattern is also evident in the frequency domain signals (Fig. 4(b) and Fig. 4(e)). While the susceptibility of the battery to electromagnetic interference may pose a concern, it is important to note that the present study involved the use of several electrical devices, a condition that may not be representative of real-world scenarios. Moreover, most data acquisition systems come equipped with built-in filter options, which can effectively address or at least diminish interference issues.

The interference of 60 Hz was drastically reduced with a notch filter. The software KiStudio Lab 2910A was used, which provides a notch filtering implementation. The transfer function of a notch filter is defined as

$$H(f) = \frac{(j2\pi f)^2 + \left(2\pi f_0\right)^2}{(j2\pi f)^2 + \left(\frac{2\pi f_0}{Q}\right)(j2\pi f) + \left(2\pi f_0\right)^2}, \tag{2}$$

where f_0 [Hz] is the notching frequency and Q is the quality factor of the filter. The notching frequency and quality factor were settled to $f_0 = 60$ Hz and Q = 83.8 (the default value in the software) for the work described in this paper. Theoretically, the effect of the notch for the frequency $f = f_{work} = 25$ Hz and its second ($f = 2f_{work} = 50$ Hz) and third ($f = 3f_{work} = 75$ Hz) harmonics are negligible, e.g., $|H(f)| \approx 1$ for $f \in \{f_{work}, 2f_{work}, 3f_{work}\}$. On the other hand, theoretically, the effect of the interference at 60 Hz results in its complete elimination, i.e., $|H(f)| \approx 0$ for $f = 60$ Hz. In practical terms, the magnitude of the transfer function was also close to unity, i.e., $|H(f)| \approx 1$ for $f \in \{ f_{work}, 2f_{work}, 3f_{work} \}$. However, $|H(f)| \neq 0$ for $f = 60$ Hz. In fact, $|H(60)| \approx 0.0041$, i.e., $|H(60)| \approx 47.6834$ dB. It must be noted that $|H(60)|$ is very low but not null. Possible explanations for $|H(60)| \neq 0$ are documented in textbooks on digital signal processing and include sampling frequencies that are not multiples of 60 Hz (its period of oscillation is a transcendental number and equal to 16.6 ms), rounding errors in the quantisation step before the analogue-to-digital conversion (ADC) process, and finite precision of the floating point operations. Nonetheless, the experimental results continue to be very good, with a substantial reduction in the signal around the 60 Hz frequency band (the time-domain signal for the 60 Hz frequency after filtering is approximately 2% of the value before filtering).

In summary, the comparison shows that the battery can generate an electrical potential difference at the same excitation frequency as the system. Also, the battery is very susceptible to noises from the electrical network (60 Hz). Therefore, it is indicated to use some type of filter in the battery signal to attenuate the noise signal due to these frequencies. The results are promising since the battery manages to generate a signal of the same frequency as the base excitation, which has many positive implications, one of which is that there is real potential for applying this type of battery in SHM systems.

3.2. Influence of the frequency and input amplitude

In the following analysis, the behaviour of the battery under a constant base excitation for different frequencies is investigated. Here, the test starts with the shaker off, and then after a few seconds, it is turned on at a constant excitation frequency and turned off again after a few seconds. For the present tests, base excitation frequencies of 15 Hz, 25 Hz and 40 Hz are used, and in all cases, the Notch filter of the acquisition system is on, and no mass is attached to the beam.

Figs. 5(a)–(c) show the battery signal in the time domain during the tests and, for each case, the regions where the shaker is off and on are highlighted. For the three cases analysed, the battery generates an oscillating variation in the electrical potential difference at a frequency of 60 Hz when the shaker is off. As previously discussed, the battery is susceptible to electromagnetic interference from the electrical network and, therefore, this behaviour is expected. In regions where the shaker is on, the battery can generate an oscillating signal at the same frequency as the base excitation, namely, 15 Hz, 25 Hz, and 40 Hz. It is important to note that the amplitude of the battery signal is considerably greater when the shaker is on. In this way, the battery can generate a representative electrical signal for the analysed cases, even with the noise coming from the electrical network.

Subsequently, the effect of input signal amplitude on the battery signal is considered. For this, three scenarios are considered:

(i) without additional mass;
(ii) mass of 30 g at the tip of the beam; and
(iii) mass of 55 g at the tip of the beam.

The frequencies of 15 Hz, 25 Hz, and 40 Hz are again used for the tests, and three measurements are taken for each case.

Table 4 shows the amplitude of the battery signal (mV) when the shaker is turned off and on. Moreover, Table 4 displays the amplitude ratio of the battery signal with the shaker both off and on. This ratio is calculated as the average of three amplitudes measured with the shaker on divided by the average of three amplitudes measured with the shaker off.

With the addition of mass to the beam, the bending strain of the beam close to the grip during the vibrational test will be greater and, consequently, this level of strain will be applied to the battery. It can be seen that both the battery signals with the shaker turned off (60 Hz) and with the shaker turned on (frequency of interest) are affected by the amplitude of the beam displacement, which is changed by the addition of mass at the beam tip.

The observed tendency indicates that, for the same base excitation frequency of the system, a higher vibration amplitude corresponds to a greater electrical response from the battery. This correlation aligns with the intuitive understanding that the piezoelectric response of materials is proportional to the strain. However, it is noticed that the amplitude ratio of the signals decreases

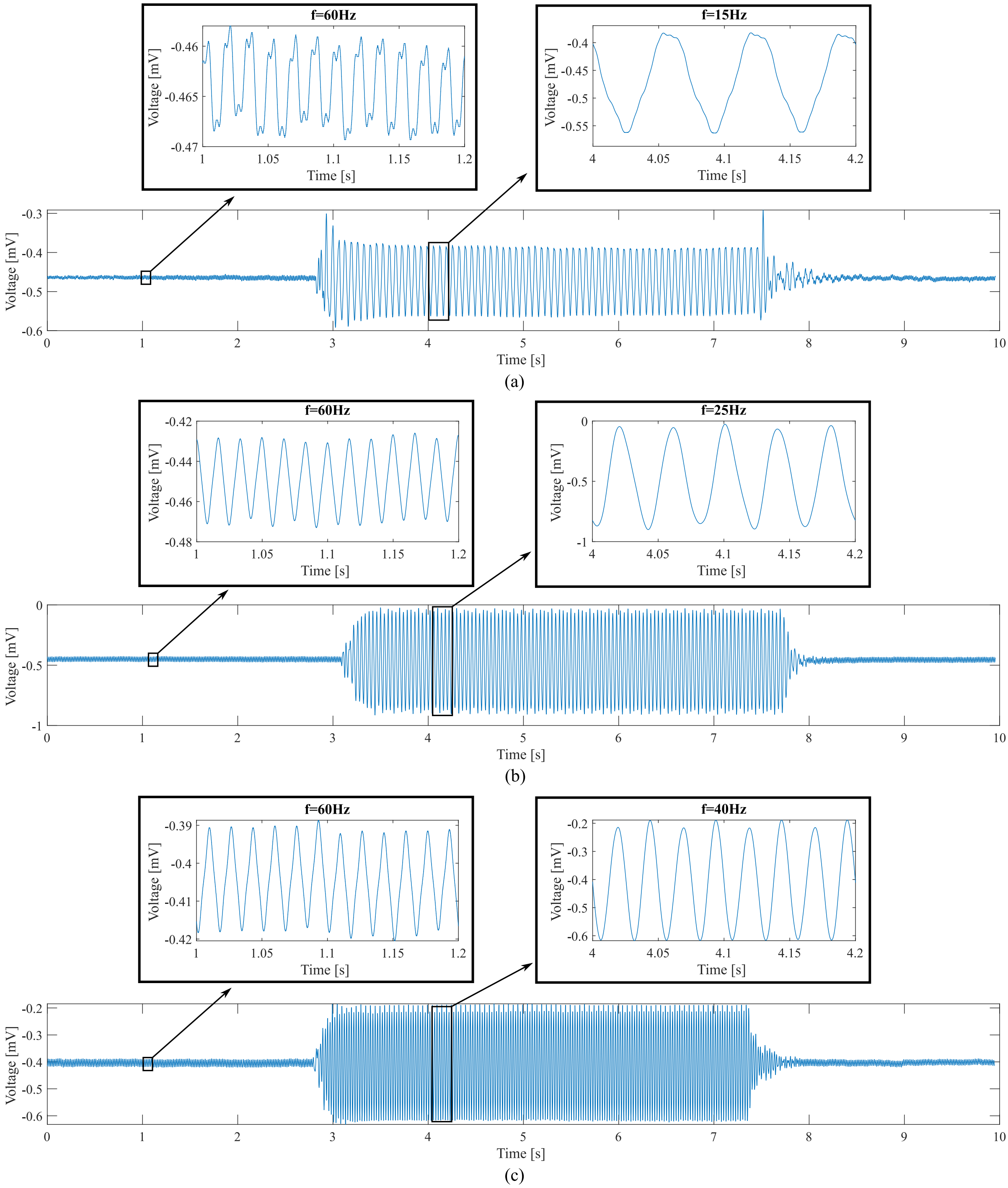

Fig. 5. Battery signal in the time domain under a constant base excitation of (a) 15 Hz, (b) 25 Hz, and (c) 40 Hz - shaker is suddenly turned on and then turned off after a few seconds - and highlights of the regions where the shaker is off and on.

as the input amplitude increases, meaning that the battery signal with the shaker turned off is more affected than the signal with the shaker turned on.

Another factor that directly influences the battery's response is the system's excitation frequency. Analysing this factor presents challenges as the vibrational amplitude of the shaker is directly influenced by the input frequency. Specifically, higher input frequencies result in lower shaker vibration amplitudes. Furthermore, the shaker-beam system exhibits an unusual behaviour within

Table 4
Comparison of battery signal amplitudes in the time domain with the shaker off (amplitude generated by the 60 Hz signal) and with the shaker on (amplitude generated by the base excitation frequency) - all data in mV -, and amplitude ratio in the signal (mean amplitude of the signal with the shaker on by the amplitude of the signal with the shaker off).

Tip mass value	Test number	15 Hz test Off	15 Hz test On	Amplitude ratio	25 Hz test Off	25 Hz test On	Amplitude ratio	40 Hz test Off	40 Hz test On	Amplitude ratio
0 g	1	0.011	0.191	12.477	0.015	0.838	32.998	0.028	0.421	15.435
	2	0.023	0.180		0.017	0.841		0.033	0.426	
	3	0.010	0.178		0.045	0.852		0.022	0.428	
30 g	1	0.032	0.290	7.826	0.057	0.873	17.097	0.056	0.162	4.125
	2	0.048	0.288		0.061	0.810		0.035	0.180	
	3	0.025	0.254		0.031	0.856		0.026	0.139	
55 g	1	0.080	0.232	3.334	0.042	0.824	12.271	0.031	0.169	2.936
	2	0.054	0.205		0.107	0.902		0.063	0.177	
	3	0.058	0.203		0.061	0.851		0.070	0.137	

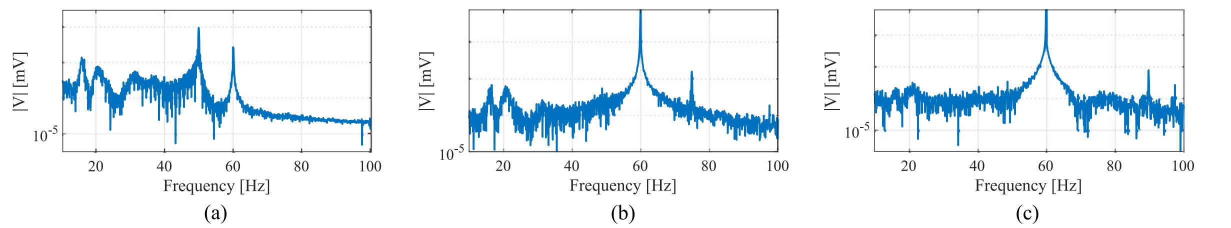

Fig. 6. Battery signal in the frequency domain for frequencies of (a) 50 Hz, (b) 75 Hz, and (c) 90 Hz. In all cases, a mass of 30 g is attached to the tip of the beam.

the frequency range of 20 Hz to 25 Hz, resembling a form of resonance. In this frequency range, increased displacement amplitude in the shaker was observed, and the results highlight that precisely at the frequency of 25 Hz, the battery generates the highest potential differences. Regarding the other two frequencies, the observed trend suggests that higher input frequencies correspond to a reduced electrical response from the battery.

Therefore, the response of the battery is influenced by both the amplitude of the base excitation and the frequency. With the setup used, it is challenging to separate these two factors since they are interdependent. Conducting a systematic case study, allowing independent control of both parameters, would be valuable to identify specific ranges where the battery operates optimally, i.e., finding a combination of frequency and amplitude where the battery generates the maximum potential difference.

Moreover, acceptable reproducibility was observed among the tests shown in Table 4, especially when considering the various uncertainties inherent in the experiments.

It is important to note that, for all cases, the battery generates a signal of considerably greater amplitude when the shaker is turned on. In the best-analysed case, the amplitude ratio is 32, while in the worst case, the amplitude ratio is approximately 3. In this way, it is possible to state that it is possible to use this type of battery to detect different levels of strain in a structure. Furthermore, since the aim was to detect the excitation frequency of the dynamic systems, the obtained results demonstrate significant potential.

3.3. Sensitivity on higher frequencies

The same tests are carried out using higher base excitation frequencies. In all cases shown, the Notch filter at 60 Hz is activated, and a mass of 30 g is used at the beam tip so that the base excitation frequencies are sufficiently far from the natural excitation frequency of the system.

At these frequencies, drawing meaningful evaluations by analysing signals in the time domain becomes challenging. Therefore, an analysis in the frequency domain is employed. Figs. 6(a)–(c) show the battery signals on the frequency domain for a constant base excitation of, respectively, 50 Hz, 75 Hz, and 90 Hz. For all cases, the amplitude of the 60 Hz peak is quite pronounced, even using the Notch filter, which attenuates this frequency. Also, the higher the base excitation frequency, the larger the difference between the 60 Hz peak and the peak at the frequency of interest.

As the frequency of the base excitation of the system increases, the displacement amplitude generated by the shaker decreases. Consequently, the strain in the beam is reduced, leading to a decrease in the signal generated by the battery. Moreover, the battery is susceptible to electrical network interference, reaching a point where this noise becomes more prominent than the response attributed to the structure's strain, even with the use of the Notch filter.

Table 5 shows the peak values of the battery signals in the frequency domain, both for the system excitation frequency and for the interference frequency. For the test at 50 Hz, it is observed that the signal amplitude at the frequency of interest is higher compared to the amplitude related to the interference. In the other two cases, the interference amplitude is greater than the amplitudes at the frequencies of interest.

Table 5
Peak values of the battery signal in the frequency domain for vibrational tests at 50 Hz, 75 Hz, and 90 Hz.

Test	Amplitude peak [mV]		Amplitude peak [mV]		Amplitude peak [mV]	
number	50 Hz	60 Hz	75 Hz	60 Hz	90 Hz	60 Hz
1	0.0094	0.0024	0.0015	0.1325	0.00078	0.1370
2	0.0105	0.0053	0.0015	0.0775	0.00077	0.0635
3	0.0099	0.0035	0.0013	0.1180	0.00060	0.1430

Table 6
Signal-to-noise ratio for vibrational tests at 50 Hz, 75 Hz, and 90 Hz.

Test	Signal-to-noise ratio [dB]		
number	50 Hz	75 Hz	90 Hz
1	11.7066	−38.4442	−44.80875
2	5.87214	−33.8560	−38.2612
3	8.9049	−38.6998	−47.5126
$\overline{\mathrm{SNR}} \pm \mathrm{SD}$	8.8279 ± 2.9180	−37.0001 ± 2.7258	−43.5275 ± 4.7568

The signal-to-noise ratio is presented in Table 6 for the vibrational tests at the three frequencies under investigation, alongside the mean values and standard deviation (SD). For the tests at a frequency of 50 Hz, the amplitude of the battery signal still exceeds the interference, albeit by a small amount of 8 dB (within the same order of magnitude). For the other cases, the dominance of the interference signal is clear, even with the filtering applied to the battery signal.

These results indicate that the batteries have limitations in monitoring higher frequencies, attributed to the small level of bending strain applied to the battery under these conditions. Hence, it is evident that the battery generates a more appropriate electrical response when subjected to greater displacement, or more precisely, larger bending strain. This observation becomes particularly noticeable when comparing the results for higher frequencies with those in Sections 3.1 and 3.2, where lower frequencies are examined, leading to more substantial bending strains applied to the battery. It is important to notice that these limitations can be overcome with the design and manufacturing of new versions of the batteries.

3.4. Remarks and perspectives

The results presented in this study represent an initial investigation into the potential and limitations of the use of a novel all-solid-state battery as a sensor. The preliminary findings are promising, suggesting a genuine opportunity for these batteries to serve as multifunctional systems, particularly as sensors for future applications in Structural Health Monitoring (SHM). The experiments revealed challenges to be overcome in the proposed use of the batteries.

The following points highlight some positive aspects identified in this study and offer perspectives on the potential use of the batteries for multifunctional applications:

- The results obtained are very promising. The proposed concept of using the batteries as sensors is feasible, as they can effectively detect the operating frequency of a dynamic system. It is worth highlighting that those batteries were not initially designed for use as sensors, but exploring this potential is considered a positive byproduct of their ferroelectric properties. Thus, in addition to their primary function, it was shown that there is great potential for the use of this type of device in multifunctional applications;
- Apart from the primary role of the batteries and their potential application as sensors demonstrated in this study, this type of battery (specifically the sodium-based electrolyte) can also be employed in structural functions, as illustrated in the work by [17]. This aspect highlights the versatility of these batteries in various applications and underscores the significance of further exploring that kind of device;
- The results obtained in this work indicate that the battery has the potential to operate as a dynamic sensor under constant frequency excitation. Considering the promising results achieved, it is anticipated that the battery might also be used to characterise the dynamic response of the structure which is attached to by means of a modal analysis - using for instance a sine sweep excitation to obtain its strain Frequency Response Function. Such result is relevant because it opens up yet another application for the batteries in terms of modal analysis and even as a smart sensor for Structural Health Monitoring (SHM) systems. As it is known, the presence of damage in a structure will result in changes in its modal parameters such as natural frequencies, vibration modes, or damping. Thus, by monitoring changes in modal parameters, the presence of damage can be inferred, as demonstrated by the authors for the case of fatigue cracks in a metallic structure [43] or even delaminations in composite plates [44]. Future research will thus be conducted to investigate the feasibility of this approach using the batteries, which could emphasise even more the multifunctional aspect of the device studied herein;
- The ferroelectric electrolyte is highly sustainable as it is fabricated from the precursors NaCl (salt) and NaOH (sodium hydroxide), which are commonly found in food and do not involve hazardous or expensive materials. The fabrication process involves wet synthesis at temperatures below 250 °C. All the precursors for the $Na_{2.99}Ba_{0.005}ClO$ ferroelectric-electrolyte are sourced from seawater. Furthermore, the batteries do not contain lithium or traditional electrode materials such as nickel

manganese cobalt oxide (NMC) or lithium iron phosphate (LFP). Instead, they utilise current collectors Zn(−) and Cu(+) serving as both collectors and electrodes. The Zn(−) can be alternatively substituted by Al(−), and Cu(+) can be substituted by Carbon(+), reducing the cell's weight and enhancing sustainability and cost-effectiveness;
- In terms of production costs, the materials used to produce the battery—electrodes, electrolyte, and protection film—are very inexpensive. However, the manufacturing process must be carried out in a dry atmosphere; otherwise, there is a risk of the electrolyte coming into contact with the atmosphere, absorbing moisture, and forming an alkaline film that might react with the electrodes, especially with zinc. Therefore, production costs can be impacted by these conditions;
- In terms of scalability and potential challenges in large-scale manufacturing, it is possible to automate the production of the batteries. For example, it is well-known that additive manufacturing processes have advanced significantly. Therefore, using a 3D printer inside a small chamber with a controlled atmosphere could be a viable alternative to produce this type of all-solid-state battery more quickly and with better process control. However, addressing this issue requires another scientific contribution.

The following points highlight some remarks and challenges encountered in the present study:

- In general, it was observed that the battery produces a better response at lower frequencies, as can be seen from the results in Sections 3.1 and 3.2 for the lower frequencies and in Section 3.3 for the higher frequencies. This is mainly because the shaker generates greater amplitudes at lower frequencies. Therefore, the vibration amplitude (which directly leads to greater bending strains in the battery) is the factor that most influences the battery response. This limitation in monitoring higher frequencies might be seen as a drawback in this version of the batteries, and new ones need to be designed and tested in future works;
- The multifunctional batteries developed by the University of Porto are manually produced, which may result in deviations in mechanical and electrical properties, potentially causing reproducibility issues. On the other hand, it is possible to design the battery as desired, for instance, changes in the materials and/or geometry parameters. However, there is still a lack of clear understanding regarding the mechanical behaviour of batteries. Given that the aim here is to evaluate the battery's response to mechanical excitation for multifunctional applications and strain sensing in structures, addressing this gap remains an open challenge;
- As for the dynamic tests presented, the base excitation amplitude does not vary linearly with frequency. The shaker-grip-beam seems to possess a natural frequency between 20 Hz and 25 Hz, leading to a higher amplitude of motion in this frequency range. Beyond this frequency range, the shaker amplitude decreases as the base excitation frequency increases. Additionally, it would be valuable to directly compare the base displacement or even the bending strain applied to the battery with its electrical response. This approach could offer an insightful evaluation of the battery;
- It is still not clear, only by the results presented in this study, if the battery has an optimal operational range. An interesting aspect to explore would involve identifying optimal points where the battery demonstrates its best performance, specifically, the point where the highest potential difference is generated. To accomplish this, it is essential to investigate the battery's response considering both the operating frequency and the amplitude of the base excitation it undergoes;
- The battery is susceptible to electromagnetic noise. However, this can be mitigated by employing Notch filters if the Q-factor is adjusted accordingly.

Finally, the main purpose of this preliminary investigation was not to fully quantify the piezoelectric behaviour of the battery when subjected to mechanical deformation but rather to present a proof-of-concept on the use of such device and further foment a discussion on the applicability of this type of multifunctional battery as a sensor. In general, the dynamic response of the battery proved to be very promising, since the amplitude of the signal generated by the battery at the tested frequencies is clearly identified.

4. Conclusion

In this work, the use of a novel all-solid-state multifunctional battery as a strain-sensing device was demonstrated. The battery is composed of a sodium-based solid electrolyte and the pair of electrodes are Copper (+) and Zinc (−). The battery is attached to an aluminium beam mounted to an electrodynamic shaker, and the battery behaviour was, for the first time, investigated under different constant base excitation frequencies.

In the initial analyses, it was shown that the battery generates a potential difference at the same frequency as the base excitation. However, the battery is very susceptible to noise from the electrical network. Thus, in addition to the base excitation frequency response, the battery also has a dynamic response at 60 Hz. To reduce this effect, a Notch filter around 60 Hz is used in all subsequent tests, thus attenuating the electrical interference. Thus, adjusting the Q-factor in the data acquisition system is crucial. The experimental results for the 25 Hz base excitation revealed a significant dominance of unfiltered 60 Hz interference at +14 dB in comparison to the unfiltered vibrational signal. However, when subjected to filtering, the amplitude of the vibrational signal surpassed the interference by +33 dB.

It can be stated that using the battery as a strain-sensing device is very promising since it generates a potential difference when excited at a constant frequency. Also, the amplitude of the signal generated by the battery when excited is easily identified, being much higher than the amplitude of the signal due to electromagnetic noise.

With the evolution of the Internet of Things and the expansion of the 4.0 industry, there is a worldwide increasing demand for both batteries and sensors. Considering the crescent concern with environmental and sustainability aspects to which engineering structures must comply, the authors believe that further investigations and development on SSE multifunctional structural batteries may pave the way to more rational and optimised use of resources without compromising the safety or performance of structures.

For future work, a sweep-type excitation signal will be used to find the natural frequencies of the system through the signal generated by the battery. Finally, aiming at Structural Health Monitoring (SHM) applications, the battery could be used to monitor damaged structures. The goal will be to determine whether the battery-generated signal could detect variations in the natural frequencies of the system resulting from the presence or absence of damage in structures. Furthermore, the discussion will address the mechanical properties of the batteries in relation to their potential for monitoring a damaged structure before battery failure. In essence, this could create opportunities for the development of self-powered Structural Health Monitoring (SHM) systems.

This emerging technology represents an advance not only in environmental aspects but also in engineering applications. It opens a new range of possibilities for the development of smart sensors fulfilling simultaneously three key features: (i) sensing, (ii) energy harvesting, and (iii) energy storage. Such a device has the potential to lead to new, efficient, lightweight, integrated, and sustainable structures.

CRediT authorship contribution statement

Bruno Guilherme Christoff: Writing – original draft, Visualization, Software, Methodology, Investigation, Formal analysis, Data curation, Conceptualization. **Denys Marques:** Writing – original draft, Visualization, Software, Methodology, Investigation, Formal analysis, Data curation, Conceptualization. **João Paulo Carmo:** Writing – review & editing, Investigation. **Maria Helena Braga:** Writing – review & editing, Investigation. **Volnei Tita:** Writing – review & editing, Supervision, Resources, Project administration, Funding acquisition.

Declaration of competing interest

The authors declare that they have no known competing financial interests or personal relationships that could have appeared to influence the work reported in this paper.

Data availability

Data will be made available on request.

Acknowledgements

Volnei Tita acknowledges the financial support of the National Council for Scientific and Technological Development (CNPq process number: 310159/2022-9). The authors are thankful for the support of the Coordination for the Improvement of Higher Education Personnel – Brazil/Finance Code 001, and for the support of Dean's Office of Researcher of the University of São Paulo via "PIPAE - PROJETOS INTEGRADOS PARA PESQUISAS EM ÁREAS ESTRATÉGICAS". M. Helena Braga acknowledges the financial support of the Portuguese Foundation for Science and Technology FCT UIDP/50022/2020 Emerging Technologies–LAETA.

References

[1] N.S. Lewis, Powering the planet, MRS Bull. 32 (10) (2007) 808–820.
[2] D. Larcher, J.-M. Tarascon, Towards greener and more sustainable batteries for electrical energy storage, Nat. Chem. 7 (1) (2015) 19–29.
[3] M. Armand, J.-M. Tarascon, Building better batteries, Nature 451 (7179) (2008) 652–657.
[4] M. Carvalho Baptista, H. Khalifa, A. Araújo, B.A. Maia, M. Souto, M.H. Braga, Giant polarization in quasi-adiabatic ferroelectric Na+ electrolyte for solid-state energy harvesting and storage, Adv. Funct. Mater. 33 (10) (2023) 2212344.
[5] J. Biemolt, P. Jungbacker, T. van Teijlingen, N. Yan, G. Rothenberg, Beyond lithium-based batteries, Materials 13 (2) (2020) 425.
[6] F. Danzi, M. Valente, S. Terlicka, M.H. Braga, Sodium and potassium ion rich ferroelectric solid electrolytes for traditional and electrode-less structural batteries, APL Mater. 10 (3) (2022) 031111.
[7] Y. Kim, W.M. Seong, A. Manthiram, Cobalt-free, high-nickel layered oxide cathodes for lithium-ion batteries: Progress, challenges, and perspectives, Energy Storage Mater. 34 (2021) 250–259.
[8] X. Zhu, S. Savilov, J. Ni, L. Li, Carbon nanoflakes as a promising anode for sodium-ion batteries, Funct. Mater. Lett. 11 (06) (2018) 1840011.
[9] Y. Wang, S. Song, C. Xu, N. Hu, J. Molenda, L. Lu, Development of solid-state electrolytes for sodium-ion battery–A short review, Nano Mater. Sci. 1 (2) (2019) 91–100.
[10] S.-W. Kim, D.-H. Seo, X. Ma, G. Ceder, K. Kang, Electrode materials for rechargeable sodium-ion batteries: potential alternatives to current lithium-ion batteries, Adv. Energy Mater. 2 (7) (2012) 710–721.
[11] J.-M. Tarascon, M. Armand, Issues and challenges facing rechargeable lithium batteries, Nature 414 (6861) (2001) 359–367.
[12] B. Scrosati, Recent advances in lithium ion battery materials, Electrochim. Acta 45 (15–16) (2000) 2461–2466.
[13] M.R. Palacin, Recent advances in rechargeable battery materials: a chemist's perspective, Chem. Soc. Rev. 38 (9) (2009) 2565–2575.
[14] B. Dunn, H. Kamath, J.-M. Tarascon, Electrical energy storage for the grid: a battery of choices, Science 334 (6058) (2011) 928–935.
[15] F. Danzi, R.M. Salgado, J.E. Oliveira, A. Arteiro, P.P. Camanho, M.H. Braga, Structural batteries: A review, Molecules 26 (8) (2021) 2203.
[16] M. Braga, J. Oliveira, A. Murchison, J. Goodenough, Performance of a ferroelectric glass electrolyte in a self-charging electrochemical cell with negative capacitance and resistance, Appl. Phys. Rev. 7 (1) (2020).
[17] F. Danzi, P.P. Camanho, M.H. Braga, An all-solid-state coaxial structural battery using sodium-based electrolyte, Molecules 26 (17) (2021) 5226.
[18] X. Feng, M. Ouyang, X. Liu, L. Lu, Y. Xia, X. He, Thermal runaway mechanism of lithium ion battery for electric vehicles: A review, Energy Storage Mater. 10 (2018) 246–267.

[19] A. Iturrondobeitia, F. Aguesse, S. Genies, T. Waldmann, M. Kasper, N. Ghanbari, M. Wohlfahrt-Mehrens, E. Bekaert, Post-mortem analysis of calendar-aged 16 Ah NMC/graphite pouch cells for EV application, J. Phys. Chem. C 121 (40) (2017) 21865–21876.

[20] J.M. Carrasco, L.G. Franquelo, J.T. Bialasiewicz, E. Galván, R.C. PortilloGuisado, M.M. Prats, J.I. León, N. Moreno-Alfonso, Power-electronic systems for the grid integration of renewable energy sources: A survey, IEEE Trans. Ind. Electron. 53 (4) (2006) 1002–1016.

[21] F. Narita, M. Fox, A review on piezoelectric, magnetostrictive, and magnetoelectric materials and device technologies for energy harvesting applications, Adv. Eng. Mater. 20 (5) (2018) 1700743.

[22] C.-W. Wu, X. Ren, W.-X. Zhou, G. Xie, G. Zhang, Thermal stability and thermal conductivity of solid electrolytes, APL Mater. 10 (4) (2022) 040902.

[23] M. Niazi, M. Valente, M.H. Braga, Structural batteries based on solid ferroelectric electrolytes, Mater. Proc. 8 (1) (2022) 151.

[24] I. El Moctar, Q. Ni, Y. Bai, F. Wu, C. Wu, Hard carbon anode materials for sodium-ion batteries, Funct. Mater. Lett. 11 (06) (2018) 1830003.

[25] C. Zhao, L. Liu, X. Qi, Y. Lu, F. Wu, J. Zhao, Y. Yu, Y.-S. Hu, L. Chen, Solid-state sodium batteries, Adv. Energy Mater. 8 (17) (2018) 1703012.

[26] H. Kim, H. Kim, Z. Ding, M.H. Lee, K. Lim, G. Yoon, K. Kang, Recent progress in electrode materials for sodium-ion batteries, Adv. Energy Mater. 6 (19) (2016) 1600943.

[27] H. Sun, P. Liang, G. Zhu, W.H. Hung, Y.-Y. Li, H.-C. Tai, C.-L. Huang, J. Li, Y. Meng, M. Angell, et al., A high-performance potassium metal battery using safe ionic liquid electrolyte, Proc. Natl. Acad. Sci. 117 (45) (2020) 27847–27853.

[28] X. Zhang, J. Meng, X. Wang, Z. Xiao, P. Wu, L. Mai, Comprehensive insights into electrolytes and solid electrolyte interfaces in potassium-ion batteries, Energy Storage Mater. 38 (2021) 30–49.

[29] L.E. Asp, M. Johansson, G. Lindbergh, J. Xu, D. Zenkert, Structural battery composites: a review, Funct. Compos. Struct. 1 (4) (2019) 042001.

[30] B.M. Gomes, J.F. Moutinho, M.H. Braga, A perspective on the building blocks of a solid-state-battery: from solid electrolytes to quantum power harvesting and storage, J. Mater. Chem. A (2023) 1.

[31] R. De Medeiros, M. Sartorato, D. Vandepitte, V. Tita, A comparative assessment of different frequency based damage detection in unidirectional composite plates using MFC sensors, J. Sound Vib. 383 (2016) 171–190.

[32] M. Sartorato, R. De Medeiros, D. Vandepitte, V. Tita, Computational model for supporting SHM systems design: Damage identification via numerical analyses, Mech. Syst. Signal Process. 84 (2017) 445–461.

[33] F.M. de Souza Mello, J.L.J. Pereira, G.F. Gomes, Multi-objective sensor placement optimization in SHM systems with kriging-based mode shape interpolation, J. Sound Vib. (2023) 118050.

[34] L.F. dos Santos Souza, D. Vandepitte, V. Tita, R. de Medeiros, Dynamic response of laminated composites using design of experiments: An experimental and numerical study, Mech. Syst. Signal Process. 115 (2019) 82–101.

[35] S. Zhou, M. Lallart, A. Erturk, Multistable vibration energy harvesters: Principle, progress, and perspectives, J. Sound Vib. 528 (2022) 116886.

[36] M. Abdulkarem, K. Samsudin, F.Z. Rokhani, M.F. A Rasid, Wireless sensor network for structural health monitoring: A contemporary review of technologies, challenges, and future direction, Struct. Health Monit. 19 (3) (2020) 693–735.

[37] G. Di Rito, M.R. Chiarelli, B. Luciano, Dynamic modelling and experimental characterization of a self-powered structural health-monitoring system with MFC piezoelectric patches, Sensors 20 (4) (2020) 950.

[38] H. Xia, Y. Xia, Y. Ye, L. Qian, G. Shi, Simultaneous wireless strain sensing and energy harvesting from multiple piezo-patches for structural health monitoring applications, IEEE Trans. Ind. Electron. 66 (10) (2018) 8235–8243.

[39] S.R. Anton, H.A. Sodano, A review of power harvesting using piezoelectric materials (2003–2006), Smart Mater. Struct. 16 (3) (2007) R1.

[40] G. Park, T. Rosing, M.D. Todd, C.R. Farrar, W. Hodgkiss, Energy harvesting for structural health monitoring sensor networks, J. Infrastruct. Syst. 14 (1) (2008) 64–79.

[41] Z. Hadas, L. Janak, J. Smilek, Virtual prototypes of energy harvesting systems for industrial applications, Mech. Syst. Signal Process. 110 (2018) 152–164.

[42] K. Group, Charge Amplifier and Data Acquisition for Multi-Channel Measurement type 5167A. URL https://www.kistler.com.

[43] D.E. Marques, D. Vandepitte, V. Tita, Damage detection and fatigue life estimation under random loads: A new structural health monitoring methodology in the frequency domain, Fatigue Fract. Eng. Mater. Struct. 44 (6) (2021) 1622–1636.

[44] R. de Medeiros, D. Vandepitte, V. Tita, Structural health monitoring for impact damaged composite: a new methodology based on a combination of techniques, Struct. Health Monit. 17 (2) (2018) 185–200.